The Astrophysical Journal Letters, 878:L16 (7pp), 2019 June 10 https://doi.org/10.3847/2041-8213/ab24d2

Using Surface Brightness Fluctuations to Study nearby Satellite Galaxy Systems: The Complete Satellite System of M101

Scott G. Carlsten[1], Rachael L. Beaton[1,2,4], Johnny P. Greco[3,5], and Jenny E. Greene[1]
[1] Department of Astrophysical Sciences, 4 Ivy Lane, Princeton University, Princeton, NJ 08544, USA; scottgc@princeton.edu
[2] The Observatories of the Carnegie Institution for Science, 813 Santa Barbara Street, Pasadena, CA 91101, USA
[3] Center for Cosmology and AstroParticle Physics (CCAPP), The Ohio State University, Columbus, OH 43210, USA
Received 2019 January 19; revised 2019 May 14; accepted 2019 May 26; published 2019 June 10

Abstract

We use surface brightness fluctuation (SBF) measurements to constrain the distance to low surface brightness (LSB) dwarfs in the vicinity of M101. Recent work has discovered many LSB candidate satellite companions of M101. However, without accurate distances, it is problematic to identify these dwarfs as physical satellites of M101. We use CFHT Legacy Survey data to measure the SBF signal for 43 candidate dwarfs. The data are deep enough that we constrain 33 of these to be unassociated background galaxies by their lack of SBF. We measure high S/N SBF signals for two of the candidate dwarfs, which are consistent with being at the distance of M101. The remaining candidates are too LSB and/or small for their distances to be constrained. Still, by comparison with Local Group dwarfs, we argue that the M101 satellite system is likely now complete down to stellar masses of $\sim 5 \times 10^5\,M_{\odot}$. We also provide a new SBF distance for the nearby dwarf UGC 8882, which suggests that it might be a physical satellite of M101; however, further study is merited. By constraining the distances to a majority of the candidates using only archival data, our work demonstrates the usefulness of SBF for nearby LSB galaxies and for studying the satellite systems of nearby massive galaxies.

Key words: galaxies: distances and redshifts – galaxies: dwarf – methods: observational – techniques: photometric

1. Introduction

Expanding the census of faint, nearby dwarf galaxies is crucial to understand structure formation on the smallest scales. In recent years this has largely been done in the form of characterizing the dwarf satellite systems of nearby ($D < 20$ Mpc) Milky Way (MW) analogs (e.g., Kim et al. 2011; Merritt et al. 2014; Bennet et al. 2017; Danieli et al. 2017; Geha et al. 2017; Müller et al. 2017; Park et al. 2017; Smercina et al. 2018) or LMC analogs (e.g., Carlin et al. 2016) with the goal of addressing the small-scale problems in ΛCDM (e.g., Bullock & Boylan-Kolchin 2017). Generally, these studies find and catalog low surface brightness (LSB) objects in deep, wide-field imaging and then either determine the distance to these objects (perhaps with follow-up spectroscopy or *Hubble Space Telescope*; *HST* observations) to confirm association with a host or group or simply assume association based on proximity on the sky. This latter assumption is very problematic for nearby systems that might be contaminated by a background group in the same area of the sky (e.g., Merritt et al. 2016; Danieli et al. 2017; Cohen et al. 2018).

In a companion paper Carlsten et al. (2019) we show that ground-based surface brightness fluctuation (SBF) measurements can efficiently provide distances and, hence, confirm association for many LSB dwarfs using the same images in which the objects were discovered. In addition, we provide an absolute SBF calibration and show that distances of 15% accuracy are possible for dwarfs as low SB as $\mu_{0i} \sim 25$ mag arcsec^{-2} in ∼1 hr exposure time with CFHT. Our calibration is well-defined over the range $0.3 \lesssim g - i \lesssim 0.8$ mag.

In this Letter, we catalog, using SBF, the dwarf companions of M101 (NGC 5457). M101 is a nearby ($D = 7$ Mpc; Lee & Jang 2012; Tikhonov et al. 2015), massive spiral galaxy with peak circular velocity of $\sim 210\,\mathrm{km\,s^{-1}}$ (Sofue 1997), which makes it a close analog in mass to the MW. It exhibits a minor pseudobulge, which contributes 3% of the luminosity (Kormendy et al. 2010), indicating a relatively merger-free history. This is corroborated by its anomalously faint stellar halo (van Dokkum et al. 2014). These features make its satellite system an interesting target of study to address predictions from structure formation models on the correlation between bulge mass and satellite abundance (e.g., López-Corredoira & Kroupa 2016; Henkel et al. 2017; Javanmardi et al. 2019).

Early studies of M101's satellite system indicated a low abundance of satellites and almost no dwarf ellipticals or dwarf spheroidals (Bremnes et al. 1999). In more recent work, the M101 satellite system has been surveyed by different groups, including using SDSS data, CFHTLS data, and two different small telescope surveys. Many LSB objects have been found and cataloged but very few have any distance constraints. In this Letter, we measure the SBF signal for many of these candidate satellites to constrain the distance, either showing them to be background or actual satellites.

This Letter is organized as follows: in Section 2 we describe the galaxy sample and data used, in Section 3 we present the SBF distance measurements, in Section 4 we discuss the results, and we summarize in Section 5.

2. Galaxy Sample and Data

We primarily use the catalog of candidate companions of Bennet et al. (2017) who used the CFHTLS. Due to the depth and resolution of the CFHTLS data, this catalog superseded the previous catalogs as it recovers all the previously discovered objects. Additionally, the detection algorithm of Bennet et al. is automated with well-understood incompleteness. This catalog includes the objects discovered by Merritt et al. (2014) and

[4] Hubble Fellow.
[5] NSF Astronomy & Astrophysics Postdoctoral Fellow.

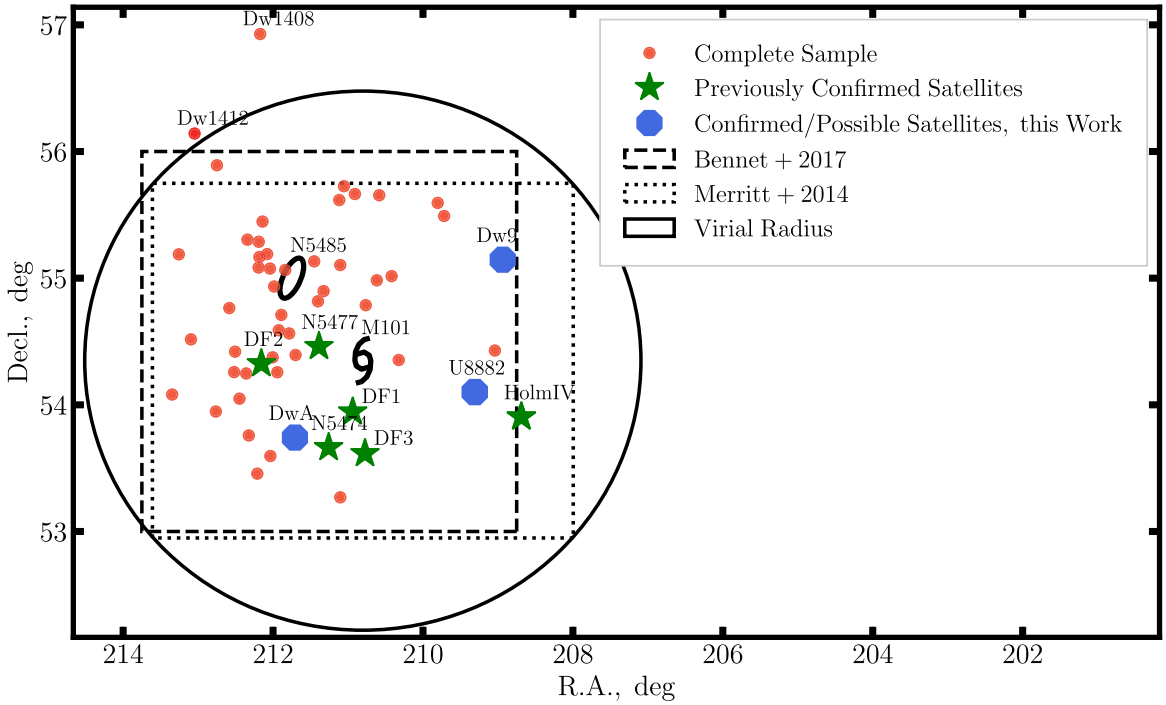

Figure 1. Sample of LSB dwarfs analyzed in this work shown relative to M101 and the background massive elliptical NGC 5485 at $D = 27$ Mpc (Merritt et al. 2014). The virial radius of M101 of 260 kpc is also shown relative to the footprints of two different surveys of the region.

Karachentsev et al. (2015),[6] in addition to several new discoveries. For completeness, we include the seven Dragonfly objects from Merritt et al. (2014) in this analysis as well even though they have distance constraints from *HST* TRGB. Danieli et al. (2017) presented *HST* TRGB distances for three of these (M101-DF1, M101-DF2, and M101-DF3), demonstrating they are at the distance of M101, and Merritt et al. (2016) showed the remaining four were at least twice the distance of M101 and likely associated with the massive elliptical NGC 5485 at a distance of 27 Mpc. However, only one of the other objects in the catalog of Bennet et al. (2017) has any distance information.[7] Two of the objects of Müller et al. (2017), dw1408+56 and dw1412+56, are in the CFHTLS footprint and we include those objects as well.

Additionally, we measure the SBF signal for the bright dwarf UGC 8882. UGC 8882 has a previous SBF distance from Rekola et al. (2005) using the calibration of Jerjen et al. (2001). We provide an updated SBF distance based on the more robust empirical calibration of Carlsten et al. (2019).

We point the reader to Table 1 of Bennet et al. (2017) for locations and properties of the candidate dwarfs. Figure 1 shows the layout of the sample relative to the footprints of the different surveys used and M101's virial radius.

We use MegaCam (Boulade et al. 2003) data from the CFHT taken as part of the Legacy Survey Wide layer. The CFHTLS-Wide data have a characteristic 50% completeness depth of 26–26.5 mag in g and 25.5–26.0 mag in i (Gwyn 2012). As discussed in Carlsten et al. (2019), the default MegaCam pipeline (Gwyn 2008) sky subtraction is unsuitable for measuring SBF of LSB objects. Instead, we download the ELIXIR (Magnier & Cuillandre 2004) preprocessed CCD-level frames from the CADC archive[8] and perform our own photometric and astrometric calibration, sky-subtraction, and stacking.

3. SBF Distances

3.1. SBF Measurement

We follow the SBF measurement methodology described in detail in Carlsten et al. (2019) which largely follows the standard SBF process (e.g., Tonry et al. 2001; Blakeslee et al. 2009; Cantiello et al. 2018). SBF is measured in the i band and the galaxy's $g - i$ color is used to account for the dependence of SBF on the stellar population. In brief, we first fit each galaxy with a Sérsic profile to model the underlying light profile. `Imfit` (Erwin 2015) is used to do the fitting. Carlsten et al. (2019) performed image simulations of LSB galaxies and found that the sky subtraction algorithm used here allowed the colors of the galaxies to be recovered with roughly 0.1 mag accuracy, which we take as a characteristic uncertainty. These smooth profile models are then subtracted from the image and we mask nearby foreground stars and background galaxies. We use `sep`[9] (Barbary 2016), a Python implementation for SExtractor (Bertin & Arnouts 1996), for the object detection. Thresholds for detection were generally in the range of 2σ–5σ above the background. The threshold was adjusted on a per galaxy basis to ensure that clear contaminating sources were always masked. These thresholds correspond to absolute magnitudes of $M_i \lesssim -4$ at the distance of M101. This ensures that star clusters associated with the galaxy are masked but the RGB tip stars in the dwarf galaxies are not.

Once masked, the images are normalized by the square root of the smooth galaxy model image and a Fourier transform is

[6] Javanmardi et al. (2016) independently discovered one of the objects (Dw A) of Karachentsev et al. (2015) using the same small-telescope data set.

[7] Dw26 of Bennet et al. (2017) is known to be $D \sim 150$ Mpc from H I observations.

[8] http://www.cadc-ccda.hia-iha.nrc-cnrc.gc.ca/en/

[9] https://github.com/kbarbary/sep

taken to calculate the power spectra. The actual region included in the Fourier transform is an ellipse centered on the galaxy that extends out to the radius where the galaxy profile drops below ~0.3 times its maximum level. The azimuthally averaged power spectrum is fit with a combination of the PSF power spectrum convolved with the mask power spectrum and a constant, representing white photometric noise.

As described in Carlsten et al. (2019), the uncertainty in the SBF measurement comes from two major sources. We estimate the uncertainty coming from the actual power spectrum fit by varying the range of wavenumbers used in the fit and the region of the galaxy used in a Monte Carlo approach. The second main source of uncertainty comes from contamination from residual, unmasked sources. For this, we measure the SBF signal in nearby background fields around each galaxy that have undergone the same normalization and masking as the galaxy. For each Monte Carlo trial, a different field is chosen at random and the residual SBF signal measured from that field is subtracted from that measured from the galaxy. We note that this approach also accounts for the effects of sky noise on the SBF measurement, which is crucial for these LSB galaxies. From this Monte Carlo approach, we get a median fluctuation level and an uncertainty from the spread in measured fluctuations.

3.2. Bounds on Distance

With measured SBF signals in hand, we turn to extracting distance information for the dwarfs in our sample. Our goal is not necessarily to determine distances for each dwarf because, as shown below, the SBF signal is very weak (or nonexistent) for most of the dwarfs, making an SBF distance impossible. Instead, the goal is to set lower bounds on the distance based on the SBF signal or lack thereof.

To determine bounds on the distance from the measured SBF signal, we use the empirical absolute calibration of Carlsten et al. (2019). We start with the measured fluctuation signal for each galaxy and propagate uncertainties in the SBF measurement and SBF calibration in a Monte Carlo approach. For each of the 10,000 iterations, we resample the SBF signal using the measured SBF signal and its uncertainty. The color of the galaxy is similarly resampled using the measured value and spread and used in the SBF calibration of Carlsten et al. (2019) to calculate the absolute SBF magnitude. Instead of using the reported error bars for the slope and zero-point of the calibration in Carlsten et al. (2019), we incorporate the uncertainty in the SBF calibration by sampling directly from the posterior distributions that come from the MCMC chains. A different zero-point and slope are drawn from the posterior distributions for each Monte Carlo trial. In this way, we deal with the strong covariance between the best-fitting slope and zero-point in the calibration (see Figure 4 of Carlsten et al. 2019). We then calculate the 2.5th, 16th, 50th, 84th, and 97.5th percentiles from the distribution of distances for each galaxy. For many of the galaxies, the resampled SBF signal could be zero or less than zero. For these galaxies, the distance distribution extends to infinity but a lower bound on the distance is still possible. Figure 2 shows these distance percentiles for each galaxy in our sample.

We note four rough groups of galaxies in Figure 2. First are the galaxies that have very wide distributions in distance but have 2σ lower bounds in distance beyond M101. We can conclude that these galaxies are background because they would have measurable SBF signal if they were at the distance of M101, which is not observed. Two examples (DwD and Dw7) are shown in Figure 3. We emphasize that concluding these galaxies are background is not a statement about the S/N of the SBF measurement. Instead, for these galaxies, if we take the measured SBF signal and add to it twice the estimated uncertainty (i.e., a 2σ upper bound), the resulting distance lower bound will still be beyond M101. Another group are the galaxies that have distance distributions extending from within M101's distance out to very large distances. These are generally the faintest and smallest galaxies of the sample and very little can be said about their distances. The S/N of the SBF measurement for these galaxies is too low for any distance constraint to be set. An example (DwC) is shown in Figure 3. A third group are the galaxies that seem to have narrow distance distributions at distances beyond M101 (e.g., Dw1408, Dw20, and Dw33). These galaxies exhibit non-Sérsic shapes and the residuals from using a Sérsic profile as a model for the smooth background could be adding spurious fluctuations into the SBF measurement. In these cases, we do not fully trust the SBF distances. The conclusion that they are beyond M101 is robust, however, because even with the added fluctuation power from an improper fit, they do not exhibit as much brightness fluctuation as they should if they were at the distance of M101. An example (Dw1408) is shown in Figure 3. The final group of galaxies are those that have narrow distance distributions (with $\pm 1\sigma$ distance ranges of $\lesssim 2$ Mpc) centered on the distance of M101. These are possibly satellites of M101 and include DwA, Dw9, Dw15, and Dw21. Of these, two are firmly at the distance of M101, see the discussion below.

There are no obvious trends between galaxy properties or exposure times and which group a galaxy ends up in. For instance, the galaxies with strong SBF signal are not the highest surface brightness or have the longest exposure times. As a simple check for how we set distance lower bounds, we performed simulations similar to those done in Carlsten et al. (2019). In short, we insert Sérsic models for the galaxies that have been resampled to have SBF into the CCD level images and reduce and analyze them in the same way as the real galaxies. We simulate DwD and Dw24 in particular as examples of galaxies that we conclude are background (one high SB and one low SB example, respectively). We run two simulations for each galaxy: one where the artificial galaxies are at a distance of 7 Mpc and one where they are at 27 Mpc (the distance of the background group). The recovered distance distributions in each case are as expected. If the artificial galaxies are placed at $D = 7$ Mpc, the recovered distances all cluster roughly at 7 Mpc. On the other hand, if they are placed at $D = 27$ Mpc, the distribution of recovered distances is much more scattered but has a 2σ lower bound beyond 7 Mpc.

We recover the distances of M101-DF1, M101-DF2, and M101-DF3 to be at the distance of M101. This agrees with the *HST* TRGB analysis of Danieli et al. (2017).[10] We are able to show that DF4, DF5, and DF6 are background but could not say anything about DF7 due to its extreme faintness. Our distance of 8.5 ± 1.0 Mpc for UGC 8882 is consistent with the distance of 8.3 ± 0.8 Mpc that Rekola et al. (2005) report.

[10] We note, however, that M101-DF1, M101-DF2, and M101-DF3 were among the galaxies used in Carlsten et al. (2019) to derive the calibration used here.

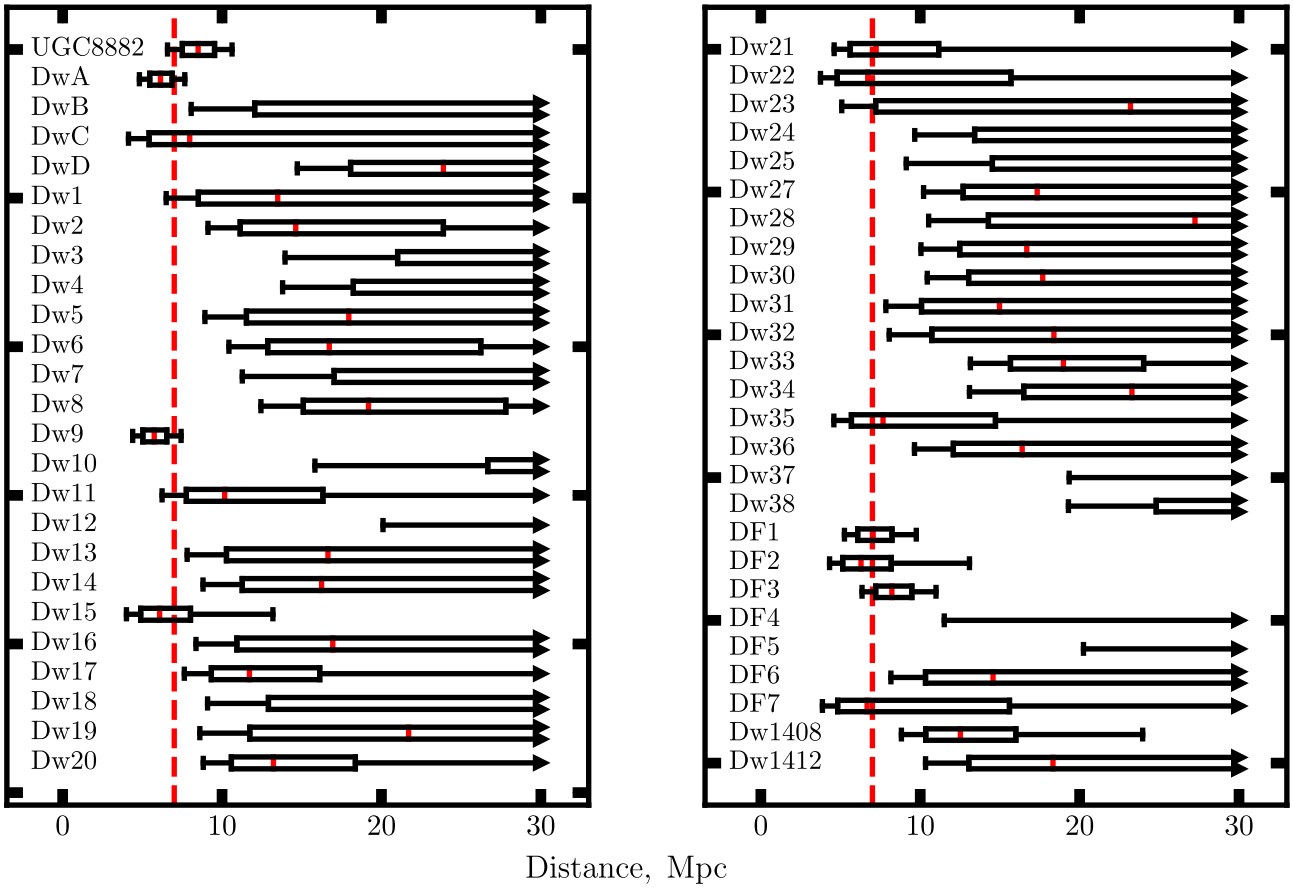

Figure 2. Box and whisker plot showing percentiles of the distance distribution that we derive for each galaxy in the sample. The whiskers extend from the 2.5th percentile to the 97.5th ($\pm 2\sigma$) and the boxes extend from the 16th percentile to the 84th ($\pm 1\sigma$). The red mark inside the boxes denotes the median. Arrows pointing to the right indicate that the distribution extends to larger distances. The dashed vertical red line at 7 Mpc indicates the distance of M101.

3.3. Confirmed Satellites

As mentioned above, four of the dwarfs appear to have significant SBF signals that put them at the distance of M101. Figure 3 shows the *i* band images of these four candidates. We note that DwA and Dw9 appear semiresolved into stars. The SBF is very strong in both galaxies (S/N of 11 and 7, respectively). The other two have weaker SBF signals (S/N $\sim$ 2–3). It is possible that the high observed fluctuation power is coming from residuals in the Sérsic fitting or, in the case of Dw21, from a single unmasked bright source in the galaxy. We take the conservative approach and include these two galaxies in the group of galaxies that do not have firm distance constraints but note they could be high priority targets for deeper follow-up. In total, out of the 43 galaxies in our sample that had no previous distance information,[11] we demonstrate that 33 are background and 2 are likely satellites of M101. For the remaining 8, we are unable to constrain the distance from the current data.

4. Discussion

4.1. Completeness of the Satellite System

To explore the properties of the galaxies on which we can set distance constraints versus those that we cannot, we plot the surface brightness and effective radii of the sample in Figure 4. The galaxies are split into three groups: those confirmed to be background with the SBF, those confirmed to be satellites with the SBF, and those where a distance constraint was not possible. The large, bright galaxies are generally those with a distance constraint, as expected. We also show the expected size and surface brightness as a function of dwarf stellar mass from the mean relations for Local Group dwarfs from Danieli et al. (2018). Most of the galaxy sample is smaller than the LG dwarfs at the same surface brightness because, as we are finding, most are background.

The curve for the LG dwarfs moves to smaller sizes and fainter surface brightness for lower stellar mass dwarfs, as expected. By comparison with the curve, it appears that the dwarf Dw9 has the lowest stellar mass of any of the confirmed satellites of $\sim 5 \times 10^5\, M_\odot$. Because we could not constrain the distance to the dwarf DwC, which has slightly fainter surface brightness than Dw9, it appears that the surface brightness and size of Dw9 is roughly the limit of the SBF technique with the current data. The SBF seems to fail for galaxies smaller than $\lesssim 4\farcs5$ and fainter than $\gtrsim 27.5$ mag arcsec^{-2}. From Figure 2 of Bennet et al. (2017), the catalog of candidate satellites should be complete at $r_{\rm eff} \sim 8''$ down to central surface brightness of $\mu_{0,\rm g} \lesssim 26$ mag arcsec^{-2}. This corresponds to a surface brightness at the effective radius of $\mu_{\rm eff,g} \lesssim 28$ mag arcsec^{-2} for the $n = 1$ Sérsics used by Bennet et al. (2017). This is fainter than the effective limit of SBF for getting a distance constraint, so the catalog of dwarfs should be complete for dwarfs of similar mass to Dw9. From this and the fact that the CFHTLS data covers most of the virial volume of M101 (see Figure 1), we

[11] Therefore not including any Dragonfly objects, Dw26, or UGC 8882.

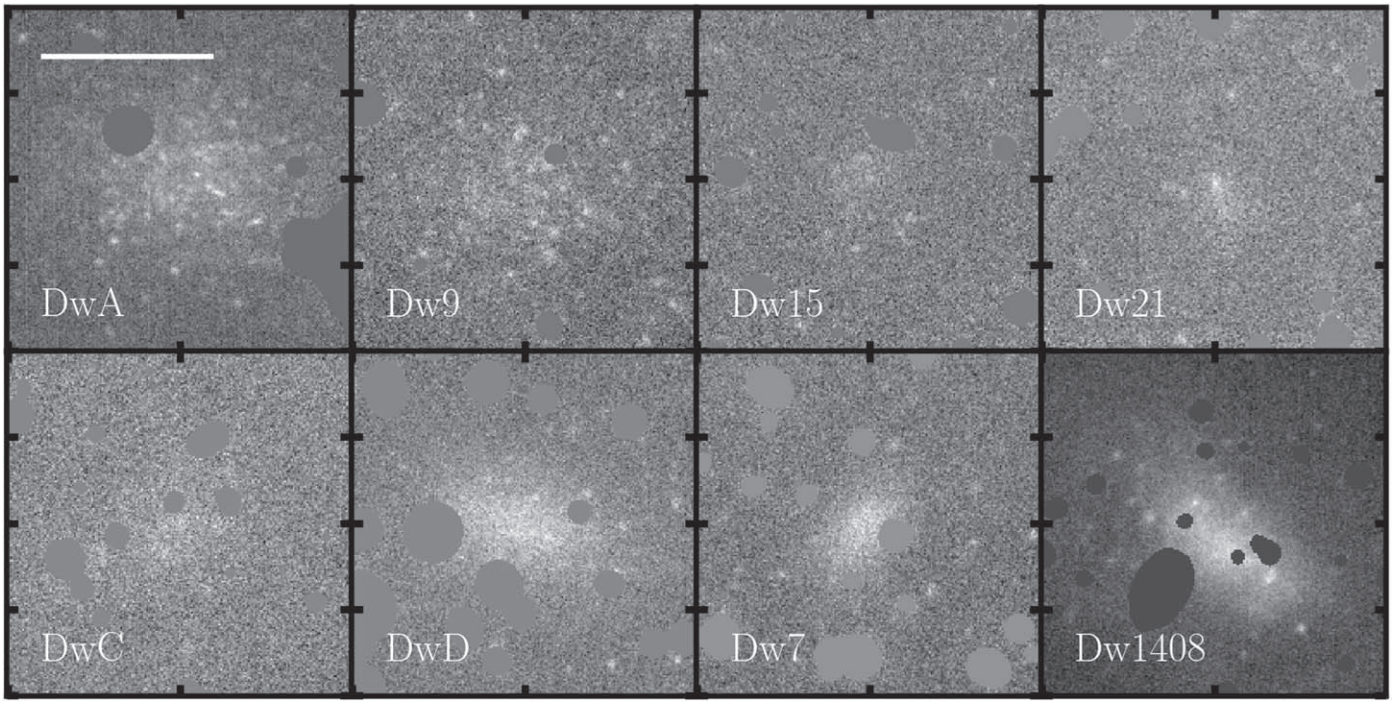

Figure 3. CFHT *i* band cutout images for a selection of the dwarf candidates, masked by the mask used in the SBF analysis. The top row are the four candidate dwarfs that have tight (±1 Mpc) distance constraints that put them at the distance of M101. The bottom row shows examples of the other cases listed in Section 3.2. DwC is an example of a galaxy that was too faint to have an SBF distance constraint. DwD and Dw7 are conclusively background. Dw1408 is conclusively background but had an SBF distance in the range of 10–15 Mpc, which is likely underestimated due to a non-Sérsic profile and profusion of contaminating point sources. The white bar in the upper left corner is 10″ (each image is at the same angular scale).

argue that the satellite system of M101 is likely now complete down to stellar masses of $\sim 5 \times 10^5\, M_\odot$.

4.2. Known Satellites

In Table 1 we list the known, confirmed satellites of M101, including the two confirmed by the current work. Our sample derives from Tikhonov et al. (2015) and Danieli et al. (2017). The first four galaxies in the table have been previously confirmed with TRGB distances and are not included in our current SBF sample. Karachentsev et al. (1994), Bremnes et al. (1999), and Müller et al. (2017) considered many more nearby galaxies as associates of M101. However, Tikhonov et al. (2015) argued that many of these members (e.g., NGC 5585 and UGC 8882) were background/foreground and physically unrelated to M101. We have found a distance of 8.5 ± 1.0 Mpc for UGC 8882, which is marginally consistent with the $D = 7$ Mpc we have used for M101. However, most of the uncertainty in the distance for UGC 8882 comes from the 0.1 mag uncertainty in color that we assume. Since UGC 8882 is so bright, this is probably overly conservative and a ±0.5 Mpc uncertainty in the distance is more realistic. Additionally, recent TRGB work (R. Beaton et al. 2019, in preparation) suggests a closer distance to M101 of ∼6.4 Mpc, which indicates that UGC 8882 might be background and not directly a satellite of M101. Still, the SBF result is ambiguous and we conclude that UGC 8882 is a possible satellite and we include it in Table 1. A more precise TRGB distance to this galaxy might be merited. We note that many of the confirmed satellites are closer than 7 Mpc with a median distance of 6.5 Mpc (not including UGC 8882) and standard deviation of 0.35 Mpc, which supports a closer distance for M101 than either the 7.24 Mpc of Lee & Jang (2012) or 6.79 Mpc of Tikhonov et al. (2015).

We include the galaxy UGC 9405 (DDO 194) in this list, but at 600 kpc from M101, it is outside of the virial radius of M101 (∼260 kpc Merritt et al. 2014). We show the currently known system in Figure 1. UGC 9405 is far off the plot to the upper left and its inclusion in the group is questionable. The other satellites exhibit an interesting asymmetry with a majority of the satellites being on one side of M101. A similar asymmetry is seen in M31 (McConnachie & Irwin 2006; Conn et al. 2013) with a significant majority of M31's satellites being on the near side of M31 to the MW.

We note there are eight known satellites of M101 with more stellar mass than $\sim 5 \times 10^5\, M_\odot$ (not including UGC 9405 or UGC 8882). The compilation of MW satellites of McConnachie (2012) includes eight MW satellites in this mass range (Canis Major, Sagittarius, LMC, SMC, Sculptor, Fornax, Leo I, and Leo II).

5. Summary

In this contribution, we have demonstrated the efficiency of using SBF measurements to constrain the distance to LSB dwarf galaxies. We have taken existing catalogs of possible dwarf satellites of the nearby spiral M101 and measured the SBF signal on the same data used in the discovery. For 33 out of the 43 dwarfs in the sample that had no previous distance constraint, we have shown that the galaxies must be background due to their lack of measurable SBF. For two galaxies in the sample, we measured SBF with high S/N, which placed them at the distance of M101. The remaining galaxies in the sample were either too faint or too small for the SBF measurement to say anything firm about the distance.

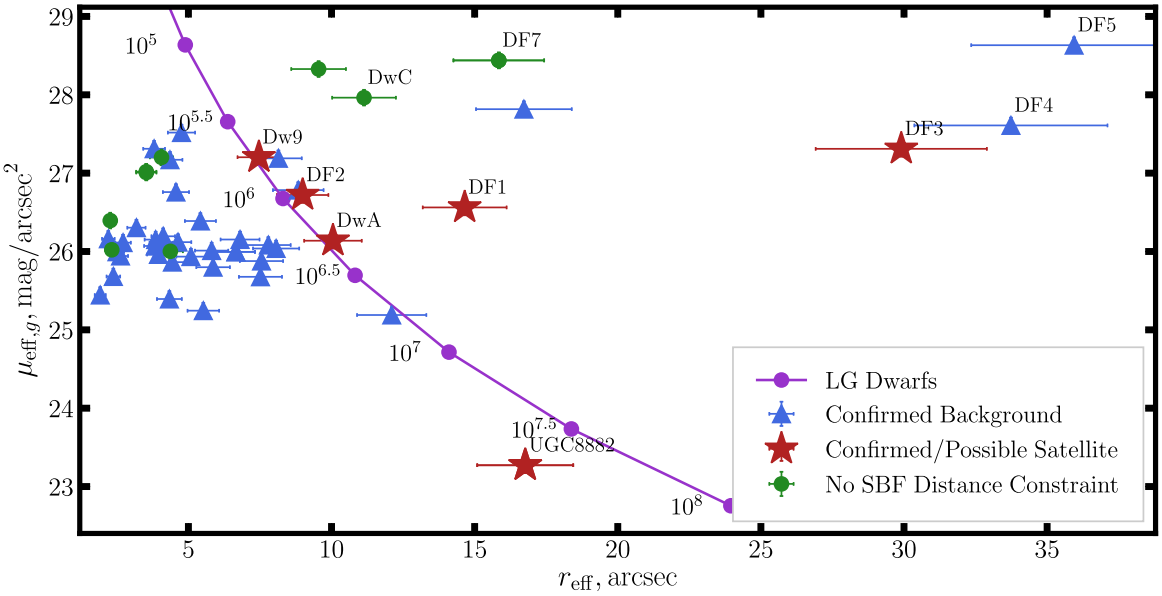

Figure 4. Surface brightness at the effective radius and effective radii of the galaxy sample, sorted by whether the SBF measurement alone could constrain them to be background or actual satellites or whether no constraint was possible. The purple curve shows the surface brightness and size for different stellar mass dwarfs (in units of $M_\odot$) from the mean relations for LG dwarfs given in Danieli et al. (2018; at the distance of M101). A 10% error in the effective radius is assumed for each point.

Table 1
Confirmed or Possible Satellites of M101

Name	R.A.	Decl.	Distance (Mpc)
NGC 5474	14:05:01.6	+53:39:44	6.82 ± 0.41 (a)
NGC 5477	14:05:33.3	+54:27:40	6.77 ± 0.40 (a)
HolmIV/UGC 8837	13:54:45.7	+53:54:03	6.93 ± 0.48 (a)
UGC 9405	14:35:24.1	+57:15:21	6.30 ± 0.38 (a)
M101-DF1	14:03:45.0	+53:56:40	$6.37^{0.35}_{0.35}$ (b)
M101-DF2	14:08:37.5	+54:19:31	$6.87^{0.21}_{0.30}$ (b)
M101-DF3	14:03:05.7	+53:36:56	$6.52^{0.25}_{0.27}$ (b)
M101-DwA	14:06:50.0	+53:44:29	6.2 ± 0.7 (c)
M101-Dw9	13:55:44.6	+55:08:45	5.8 ± 0.8 (c)
UGC 8882	13:57:14.7	+54:06:03	8.5 ± 1.0 (c)

References. (a) Tikhonov et al. (2015); (b) Danieli et al. (2017); (c) current work.

Since we utilized the same data set used in discovering the dwarfs, we avoided the need for follow-up to determine distances. If TRGB were used, *HST* follow-up would likely be required, which for 43 candidates with limited multiplexing and 1–2 orbits per object would be very expensive. At the same time, the fact that at least 33 out of the 43 dwarf candidates are background objects highlights the need for distance measurements when studying the satellite systems of nearby galaxies.

By comparison with the size and surface brightness of LG dwarfs, we argued that SBF distance constraints were possible with these data down to stellar masses of $\sim 5 \times 10^5\, M_\odot$. Bennet et al. (2017) showed that the candidate catalog is complete at this size and surface brightness. Therefore, since the CFHTLS data used covers most of the virial volume of M101, we argued that the satellite system of M101 is likely complete down to roughly this mass. Table 1 lists the known members. This completeness will make M101 useful in confronting predictions from structure formation theories on expected satellite abundance and properties.

Finally, we mention that this sort of analysis will be very useful in the future with large surveys like the Hyper Suprime-Cam[12] (Aihara et al. 2018) and LSST. The combined depth and wide area of these surveys will facilitate the discovery of many LSB objects (e.g., Greco et al. 2018a, 2018b). Follow-up with *HST* or *JWST* for everything discovered will not be possible, but the depth and quality of the survey imaging will make the SBF approach, like we used here, very feasible.

Support for this work was provided by NASA through Hubble Fellowship grant #51386.01 awarded to R.L.B. by the Space Telescope Science Institute, which is operated by the Association of Universities for Research in Astronomy, Inc., for NASA, under contract NAS 5-26555. J.P.G. is supported by an NSF Astronomy and Astrophysics Postdoctoral Fellowship under award AST-1801921. J.E.G. and S.G.C. are partially supported by the National Science Foundation grant AST-1713828.

Based on observations obtained with MegaPrime/MegaCam, a joint project of CFHT and CEA/IRFU, at the Canada–France–Hawaii Telescope (CFHT), which is operated by the National Research Council (NRC) of Canada, the Institut National des Science de l'Univers of the Centre National de la Recherche Scientifique (CNRS) of France, and the University of Hawaii. This work is based in part on data products produced at Terapix available at the Canadian Astronomy Data Centre as part of the Canada–France–Hawaii Telescope Legacy Survey, a collaborative project of NRC and CNRS.

ORCID iDs

Scott G. Carlsten https://orcid.org/0000-0002-5382-2898
Rachael L. Beaton https://orcid.org/0000-0002-1691-8217
Johnny P. Greco https://orcid.org/0000-0003-4970-2874

[12] https://hsc.mtk.nao.ac.jp/ssp/

References

Aihara, H., Arimoto, N., Armstrong, R., et al. 2018, PASJ, 70, S4
Barbary, K. 2016, JOSS, 1, 58
Bennet, P., Sand, D. J., Crnojević, D., et al. 2017, ApJ, 850, 109
Bertin, E., & Arnouts, S. 1996, A&AS, 117, 393
Blakeslee, J. P., Jordán, A., Mei, S., et al. 2009, ApJ, 694, 556
Boulade, O., Charlot, X., Abbon, P., et al. 2003, Proc. SPIE, 4841, 72
Bremnes, T., Binggeli, B., & Prugniel, P. 1999, A&AS, 137, 337
Bullock, J. S., & Boylan-Kolchin, M. 2017, ARA&A, 55, 343
Cantiello, M., Blakeslee, J. P., Ferrarese, L., et al. 2018, ApJ, 856, 126
Carlin, J. L., Sand, D. J., Price, P., et al. 2016, ApJL, 828, L5
Carlsten, S., Beaton, R., Greco, J., & Greene, J. 2019, arXiv:1901.07575
Cohen, Y., van Dokkum, P., Danieli, S., et al. 2018, ApJ, 868, 96
Conn, A. R., Lewis, G. F., Ibata, R. A., et al. 2013, ApJ, 766, 120
Danieli, S., van Dokkum, P., & Conroy, C. 2018, ApJ, 856, 69
Danieli, S., van Dokkum, P., Merritt, A., et al. 2017, ApJ, 837, 136
Erwin, P. 2015, ApJ, 799, 226
Geha, M., Wechsler, R. H., Mao, Y.-Y., et al. 2017, ApJ, 847, 4
Greco, J. P., Greene, J. E., Price-Whelan, A. M., et al. 2018a, PASJ, 70, S19
Greco, J. P., Greene, J. E., Strauss, M. A., et al. 2018b, ApJ, 857, 104
Gwyn, S. D. J. 2008, PASP, 120, 212
Gwyn, S. D. J. 2012, AJ, 143, 38
Henkel, C., Javanmardi, B., Martínez-Delgado, D., Kroupa, P., & Teuwen, K. 2017, A&A, 603, A18
Javanmardi, B., Martinez-Delgado, D., Kroupa, P., et al. 2016, A&A, 588, A89
Javanmardi, B., Raouf, M., Khosroshahi, H. G., et al. 2019, ApJ, 870, 50
Jerjen, H., Rekola, R., Takalo, L., Coleman, M., & Valtonen, M. 2001, A&A, 380, 90
Karachentsev, I. D., Kopylov, A. I., & Kopylova, F. G. 1994, BSAO, 38, 5
Karachentsev, I. D., Riepe, P., Zilch, T., et al. 2015, AstBu, 70, 379
Kim, E., Kim, M., Hwang, N., et al. 2011, MNRAS, 412, 1881
Kormendy, J., Drory, N., Bender, R., & Cornell, M. E. 2010, ApJ, 723, 54
Lee, M. G., & Jang, I. S. 2012, ApJL, 760, L14
López-Corredoira, M., & Kroupa, P. 2016, ApJ, 817, 75
Magnier, E. A., & Cuillandre, J.-C. 2004, PASP, 116, 449
McConnachie, A. W. 2012, AJ, 144, 4
McConnachie, A. W., & Irwin, M. J. 2006, MNRAS, 365, 902
Merritt, A., van Dokkum, P., & Abraham, R. 2014, ApJL, 787, L37
Merritt, A., van Dokkum, P., Danieli, S., et al. 2016, ApJ, 833, 168
Müller, O., Scalera, R., Binggeli, B., & Jerjen, H. 2017, A&A, 602, A119
Park, H. S., Moon, D.-S., Zaritsky, D., et al. 2017, ApJ, 848, 19
Rekola, R., Jerjen, H., & Flynn, C. 2005, A&A, 437, 823
Smercina, A., Bell, E. F., Price, P. A., et al. 2018, ApJ, 863, 152
Sofue, Y. 1997, PASJ, 49, 17
Tikhonov, N. A., Lebedev, V. S., & Galazutdinova, O. A. 2015, AstL, 41, 239
Tonry, J. L., Dressler, A., Blakeslee, J. P., et al. 2001, ApJ, 546, 681
van Dokkum, P. G., Abraham, R., & Merritt, A. 2014, ApJL, 782, L24